small method
www.small-methods.com

Multiscale Microstructure for Investigation of Cell–Cell Communication

*Ann-Kathrin Schneider, Tim Scharnweber, Destiny Cammann, Bastian Rapp, Stefan Giselbrecht, and Christof M. Niemeyer**

A multiscale polydimethylsiloxane (PDMS) chip is presented, which provides an array of mesoscale open wells for cell culturing and, as unique feature, an array of microscale 1 µm deep channels to fluidically connect neighboring wells. As demonstrated with SH-SY5Y cells, the small dimensions of the channels prevent migration of the cell soma but allow physical contacts established by the outgrowth of protoplasmic protrusions between cells in adjacent wells. Another important feature is the chip's mountability on solid substrates, such as glass. This enables the use of substrates previously patterned with biomolecules, as demonstrated by DNA-directed immobilization of proteins inside the reactor wells. Given the versatile addressability of cells, whether through surface-bound or inkjet-based administration of bioactive substances, it is believed that the reactor could be used for research in cell–cell communication networks, for example, in neurodegenerative diseases such as Alzheimer's disease.

1. Introduction

Bioreactors are essential tools for advanced cell biology and biotechnology applications and have proven to be an indispensable tool for maintaining well-controlled microenvironments for cultivation, differentiation, stimulation, and analysis of living cells.[1] A prominent example in this regard is mimicking stem cell niches in vitro, which enable cultivation, self-renewal, and directed differentiation of these cells.[2] There is currently a strong focus on the development of bioreactor systems for neuronal cells, with the aim of gaining a deeper understanding of the origin and progression of cellular dysfunction associated with neurodegenerative diseases such as Alzheimer's disease (AD).[3]

Although the essential role of intra- and extracellular deposition of misfolded proteins such as Tau and amyloid-β in these diseases has been identified, which lead to an interruption or restriction of axonal transport, the underlying molecular mechanisms of the plaques formed are still largely unclear.[4] As life expectancy continues to rise, more than 16 million people in Europe are expected to have Alzheimer's in 2050,[5] there is a high demand for reliable and stable in vitro methods and bioreactor platforms to perform basic research and applied drug testing.

Existing bioreactor systems are often based on polydimethylsiloxane (PDMS), which allows the easy fabrication of 2D and 2.5D structures by soft lithography.[6] However, simple molding processes offer few possibilities for the integration of interconnected but yet specifically addressable compartments in which individual cells and cell populations can be cultured. The investigation of intercellular processes, such as axonal transport, for example, would require a compartmentalized bioreactor consisting of individual, interconnected compartments in which cells are cultured spatially separated from each other, but can still communicate with each other through narrow channels. Furthermore, the compartments should be addressable from the outside, so that they can, for example, be loaded with different bioactive substances. Ideally, the compartments should also be individually modifiable with regard to their surface chemistry, for example, to immobilize different bioactive components on the surface.

In order to establish a microstructure system that allows both spatially separated cocultivation and the specific treatment of cells within a well with immobilized or dissolved bioactive factors, we report here on a two-scale microstructure that contains wells in the surface of a polymer body with different depths and can be bonded to functionalized glass surfaces. The fabrication method developed for this purpose leads to first recesses with a depth of 150 µm (200 × 200 µm width/length)

Dr. A.-K. Schneider, Dr. T. Scharnweber, D. Cammann, Prof. C. M. Niemeyer
Karlsruhe Institute of Technology (KIT)
Institute for Biological Interfaces (IBG 1)
Hermann-von-Helmholtz-Platz 1
Eggenstein-Leopoldshafen D-76344, Germany
E-mail: niemeyer@kit.edu
Prof. B. Rapp
Laboratory of Process Technology | NeptunLab
Department of Microsystems Engineering (IMTEK)
Albert-Ludwigs University of Freiburg
Georges-Köhler-Allee 103, Freiburg im Breisgau D-79110, Germany
Dr. S. Giselbrecht
MERLN Institute for Technology-Inspired Regenerative Medicine
Maastricht University
Universiteitssingel 40, Maastricht ER 6229, The Netherlands
The ORCID identification number(s) for the author(s) of this article can be found under https://doi.org/10.1002/smtd.202000647.

DOI: 10.1002/smtd.202000647

and a second type of recesses with a depth of only 1–2 µm (7 × 200 µm width/length). After bonding the polymer body to the glass substrate, the first recesses are opened to create wells for holding sample fluids or biological cells, and the second recesses are used to create channels that fluidically connect the wells.

While the surface immobilization of bioactive components for specific cell stimulation is usually limited to the complete bioreactor and is done either by simple physisorption[7] or chemical methods,[8] the unique design of our microreactor allows for using the site selective DNA-directed immobilization (DDI) of proteins[9] to assemble patterned protein surfaces inside individual wells. We demonstrate this patterning approach using glass surfaces equipped with DNA oligonucleotides as solid support for the PDMS chip, thereby allowing the site-specific immobilization of protein–DNA conjugates inside the reactor's wells. We illustrate the usefulness of our reactor for cultivation of neuronal progenitor cells, the widely used SH-SY5Y neuroblastoma cell line,[10] and their differentiation in individual wells. The formation of cell–cell contacts through interconnecting channels of adjoining wells was observed by live cell imaging during the differentiation procedure. To demonstrate the possibility of specific cell stimulation, living cells were also selectively stained and monitored by fluorescence microscopy over several hours. Altogether, the results indicate that our reactor design enables the specific cell treatment in particular wells both with solved and immobilized molecular factors.

2. Results and Discussion

2.1. Fabrication of the Microreactor

The microreactor was designed and fabricated to offer 100 wells (dimensions: $L/H/W$ 200 × 150 × 200 µm), interconnected by small channel structures (dimensions: $L/H/W$ 200 × 1 × 7 µm). The array of interconnected wells is surrounded by a 2.5 mm wide frame serving as a medium reservoir (Figure S1, Supporting Information). The reservoir itself is also connected to the outer wells by the small channels and can hold a volume of 20 µL cell culture media, which is sufficient to supply the wells with media through the channel structures (**Figure 1**B,C). To limit evaporation in individual wells, we additionally established an incubation chamber, which can be put on top of the microreactor. This incubation chamber has been designed for a volume of 200 µL water and limits the volume above the microreactor when a sealing slide is placed on top (Figure 1A). The chamber itself is made of PDMS and thus seals automatically when mounted onto the microreactor. The fact that no bonding is required has the advantage that the reactor can be easily removed from the incubation chamber later. This reversible assembly allows access to biological samples at a later time, e.g., to harvest cells for single cell studies.

In order to develop the desired microstructure, we initially established a suitable multistep fabrication process. The challenge was to produce a PDMS chip with structures of different heights. The wells should be as deep as possible to provide

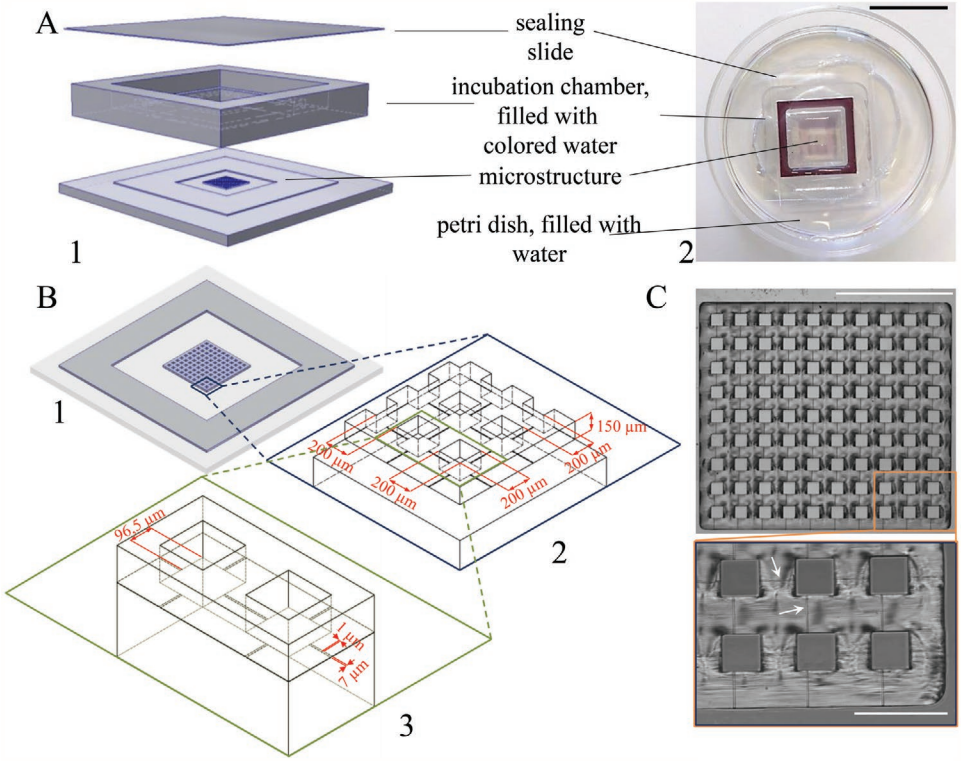

Figure 1. Dimensional drawing of the two-scale microstructure. A-1) Schematic illustration of the complete setup including 2) the microreactor, the incubation chamber, and a sealing slide as well as a photographic image thereof (scale bar: 25 mm). B-1) Microchip structure and 2) dimensions of wells, and 3) interconnecting channels. C) Microscopy image of the microreactor (top view, scale bar: 2 mm) and magnified area containing six wells (scale bar: 500 µm). The arrows indicate interconnecting channels.

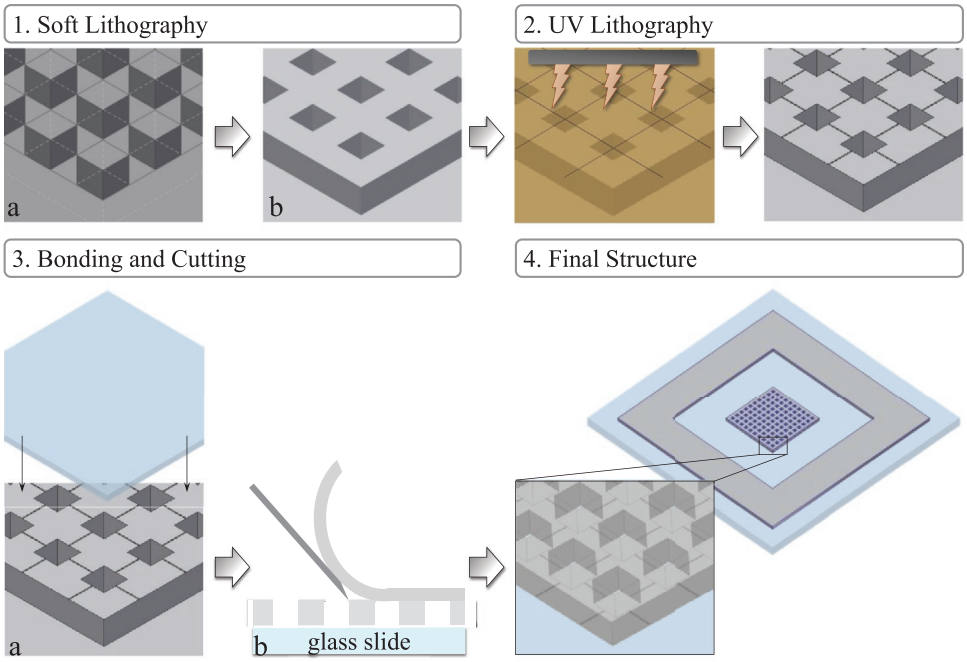

Figure 2. Overview of the microreactor fabrication process. 1a) The first step includes soft lithographic molding of a negative master featured with the basic array of wells and the surrounding frame structure. 1b) The resulting PDMS cast is micro patterned by UV lithography to generate the 2) interconnecting channel structures. 3a) The patterned PDMS is then activated by oxygen plasma and bonded with the structured face directly onto a glass slide. 3b) To open the top of the wells, the PDMS is cut slice-by-slice from the top using a vibratome (cross section of the microchip is shown). 4) The final structure contains a PDMS layer with 100 wells interconnected by small channel structures, which are located directly on the glass surface.

sufficient amounts of medium for the cell culture, while the connecting channel structures should have the lowest possible height to prevent the cell bodies from migrating. A possible cell migration depends mainly on physical material properties and the deformability of the cells. The size and stiffness of the cell nucleus are the main factors that determine whether migration can occur.[11] For SH-SY5Y cells, it was found that a pore diameter around 1.2 µm effectively prevents cell migration.[12] Furthermore, it is established that 7 μm^2 is a safe cross-sectional area to prevent cell body migration.[13] Since the width of the channels was limited to about 7 µm by the lithography step described in the following, channel structures of about 1 um depth were created with this method to prevent the migration of cell bodies between the wells but still allow cell–cell physical contacts. To meet this challenge, we combined and optimized soft and UV lithography steps, resulting in a novel manufacturing strategy that enabled the production of the designed microstructure. An overview of the established workflow is shown in **Figure 2**. It starts with the fabrication of a PDMS chip, in which the deep recesses of the microreactor, i.e., the wells and the surrounding frame structure, were introduced by means of soft lithography.

The resulting PDMS chip was then further processed via UV lithography[14] to integrate the interconnecting channel structures. For this purpose, a gold coated quartz glass patterned with an UV permeable grid of 5 µm wide lines, in the following referred to as gold mask, was used. Irradiation of the PDMS chip with 185 nm UV light through the gold mask and subsequent development by treatment with aqueous NaOH resulted in the formation of the desired channel structures (about 1.2 × 7 µm in depth and width, respectively). Further treatment with oxygen plasma led to enhanced surface hydrophilicity of the PDMS to aid the bonding of the chip with its structured face directly onto the glass surface. The final production step included the slice-by-slice cutting of the PDMS from top by using a vibratome to open the wells and to make them accessible from top. A detailed description of the experimental development of the microreactor fabrication process, which included optimization of casting molds, trials of replica production by thermoforming and double casting as well as post-fabrication treatments to optimize hydrophilicity and biocompatibility, is given in chapter 1 and Figures S2–S10 of the Supporting Information.

2.2. Functional Characterization of the Microreactor

Prior to cell culture experiments, the basic functionality of the microreactor, manufactured as described above, was investigated to show that the established structure allows cell stimulation by both immobilized and dissolved reagents.

First, a proof of concept for the selective immobilization of different reagents within the reactor's wells by means of DNA directed immobilization was demonstrated (**Figure 3**). Since a glass surface forms the bottom of the wells, the DNA capture oligonucleotides required for this can be easily immobilized using well-established protocols based on silane chemistry.[9b] We used the initial functionalization of a microscopy glass slide surface with aminopropyl-triethoxysilane (APTES) to which a layer of bis-epoxy-poly(ethylene glycol) (EPEG) was then covalently bound. All experimental protocols are detailed in chapter 2 of the Supporting Information. Subsequently, a pattern of

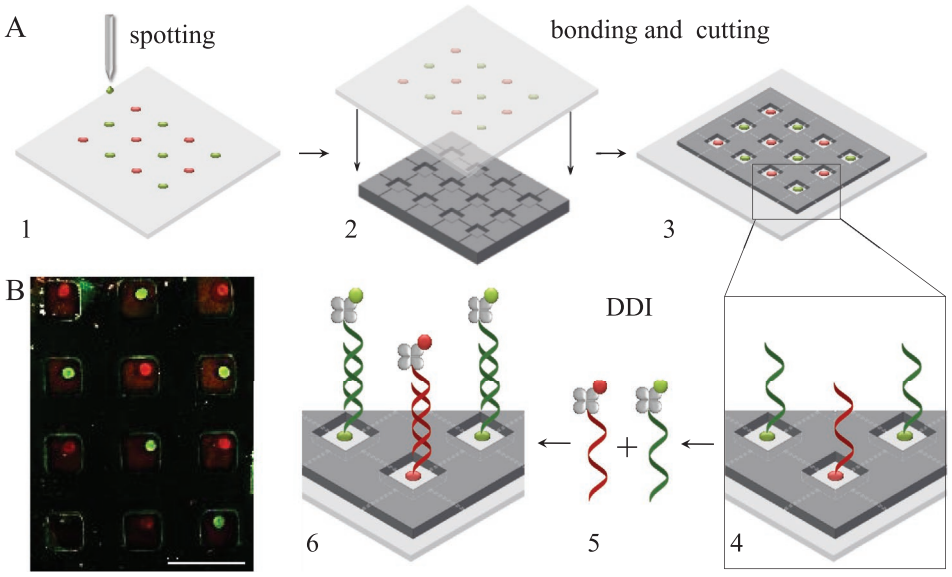

Figure 3. DNA-directed immobilization (DDI) of two different atto dye-labeled protein–DNA conjugates inside the wells of the microreactor. A) Schematic illustration of the workflow. Capture oligonucleotides (aF1 in green, aF9 in red) are spotted in an alternating pattern on a 1) chemical activated glass surface, 2) the PDMS chip is bonded on the glass slide, and 3) the wells are opened by vibratome cutting. 4) The now accessible wells are filled with a mixture of 5) two DNA-streptavidin (STV) conjugates, cF1-bio-atto550 (green), and cF9-bio-atto647 (red), 6) to allow for site-selective binding by hybridization with the corresponding capture oligomers on the surface. B) Fluorescence microscopy image of the resulting well array. Immobilized atto550 and atto647 labels are indicated by green and red spots, respectively. Scale bar: 400 µm.

alternating spots of two aminoalkyl-derivatized 21-mer DNA oligomers (aF1, aF9, for sequences, see Table S1 in the Supporting Information) was installed by ink-jet microdeposition. The so-functionalized glass slide was then aligned and bonded to the microstructured PDMS chip, such that the DNA spot micropatterns were located inside the wells. The correct alignment of the PDMS chip was monitored with a light microscope. As depicted in the workflow of Figure 3A, the wells were then opened by vibratome cutting and used as reaction vessels for DNA-directed immobilization of DNA-protein conjugates.

To this end, covalent conjugates were prepared from streptavidin (STV) and two different single-stranded oligonucleotides (cF1, cF9) complementary to the surface-bound capture sequences. In separate reactions, the two conjugates were labeled with distinguishable biotinylated fluorophores (bio-atto550 or bio-atto647, green and red spots, respectively, in Figure 3B). Subsequently, an equimolar mixture of the two conjugates (cF1-STV-bio-atto550, cF9-STV-bio-atto647) was prepared and the reactor was overlaid with this solution such that all wells were filled. Following to incubation for 60 min, the reactor was washed to remove unbound material and analyzed by fluorescence imaging (Figure 3B). The results clearly revealed the expected alternating pattern of green and red spots inside the wells that was formed by specific DNA-directed immobilization. Of note, no fluorescent signal was observed in the areas surrounding the DNA spots. This clearly shows that the immobilization was exclusively due to the specific Watson–Crick base pairing. Due to this high specificity of DDI,[9b] it should therefore be possible to immobilize many different protein reagents in the different wells of the reactor. In addition, this approach also enables nanostructured protein assemblies to be presented specifically on the surface for growing cells.[15]

Next, we investigated the distribution of fluids through the channel structures of the PDMS microreactor. When the PDMS surface was previously hydrophilized by extraction and subsequent treatment with PEG silane, addition of medium into the outer frame structure was sufficient to fill all wells within ≈12 h by capillary forces. In the case of untreated surfaces, however, no filling takes place (Figure S11, Supporting Information). To avoid the 12 h incubation time and to enable fast working, the entire reactor was covered with an excess volume of medium for the following experiments, which was then removed so that only the wells of the reactor were filled with medium.

To mimic cell-based screening assays and to investigate whether a distribution of small molecules can occur by diffusion through the channels of adjacent wells, we added a small volume (5 droplets of each 300 pL) of the bio-atto550 fluorescent dye to an individual well of the reactor previously filled with media and tracked the resulting distribution of the fluorescence signal over time (**Figure 4** and Figure S13B, Supporting Information). While no substantial increase in fluorescence was observed in the adjacent wells after 5 h, we found a strong accumulation of the fluorescent molecule at the interface of the well and two outgoing channels. The uneven distribution of the fluorescence signals in the channels in Figure 4B is probably due to the fact that the two weakly fluorescing channels have a smaller diameter and are therefore discontinuous and/or poorly wettable. In order to investigate the basic quality and reproducibility of chip manufacturing, a statistical analysis of the channel depths was performed (Figure S6, Supporting Information). The obtained results showed a uniform distribution of channel depths, however, chip-to-chip variances and outliers were also observed. In addition, the fluorescence intensity in well A changed over time from a uniformly distributed

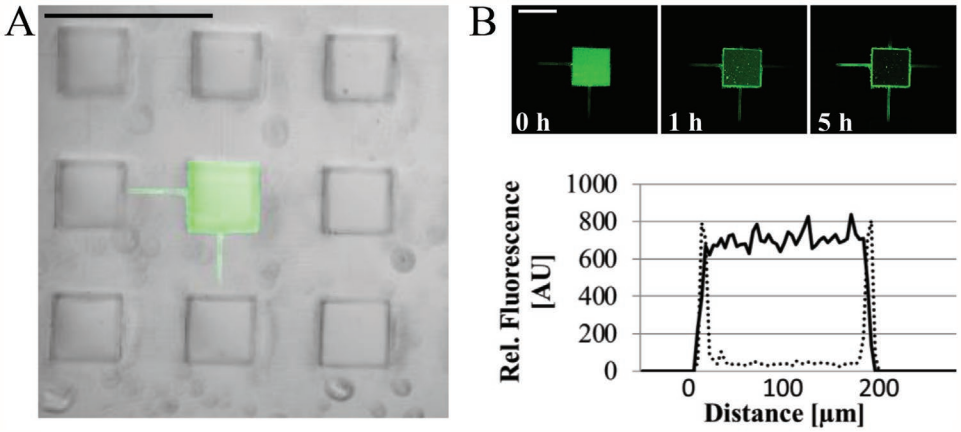

Figure 4. Addition and distribution of a small molecule in the assembled microreactor. Bio-atto550 (green) was used as a hydrophobic model drug and spotted into a single well of the reactor previously filled with media. The distribution of the fluorescence was analyzed over 5 h at 37 °C. Note that the uneven distribution of fluorescence signals in the four channels is probably due to the fact that the two weakly fluorescent channels have a smaller diameter and are therefore discontinuous and/or poorly wettable. For a statistical analysis of the channel depths, see Figure S6 in the Supporting Information. A) Microscopy image merged of bright field and fluorescence at $t = 0$ h. Scale bar: 500 µm. B) Upper pictures: fluorescence images of the central well at different time points. Scale bar: 200 µm. Lower chart: Distribution of the fluorescence signal (emission at 575 nm) in the central well at $t = 0$ h (black line) and $t = 5$ h (dotted line). Note that the hydrophobic Bio-atto550 dye shows a rapid decrease of the fluorescence signal in the center of the well due to adsorption to the PDMS surface, leading to an increase in fluorescence at the walls of the well.

signal to a strong decrease in the center and a strong accumulation at the edges of the well (Figure 4B). These results show that strongly hydrophobic molecules, such as the bio-atto550 used here, absorb to a high degree to the hydrophobic PDMS surface, as has been frequently reported in other studies.[16]

Similar results were obtained with another low-molecular hydrophobic dye, MitoTracker Green (**Figure 5**). While the addition of this dye led to the desired specific staining of the cells, no significant diffusion into neighboring wells of the dye took place, so that after 5 h a maximum signal of <5% was observed in the adjacent wells (Figure S13D, Supporting Information). These results demonstrate that the targeted addition of substances into specific wells can be used to stimulate cells with lipophilic molecules over several hours. This is not

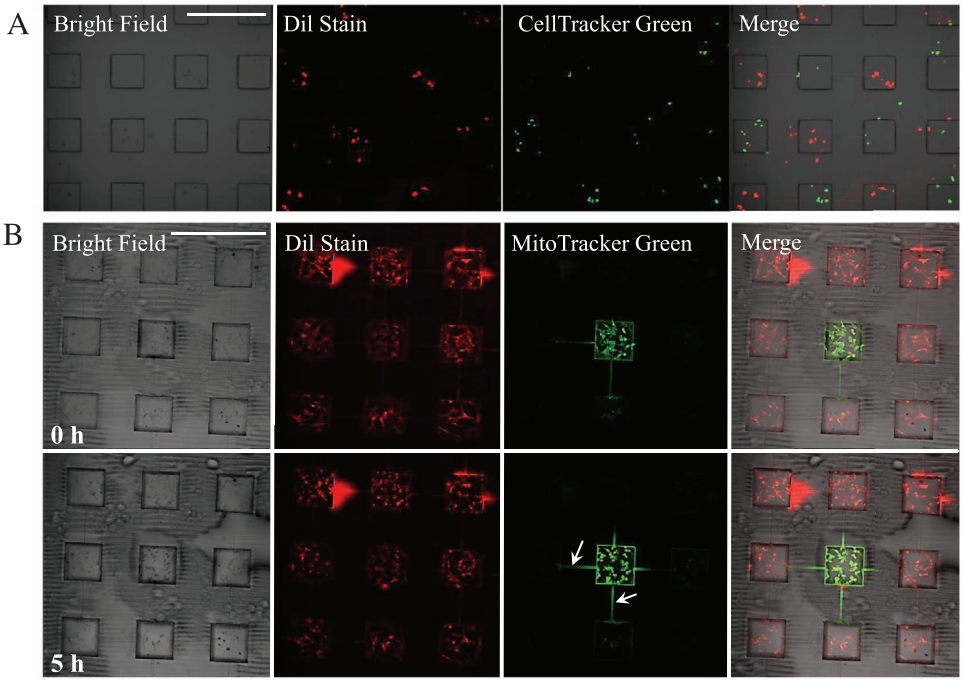

Figure 5. Spotting of cells and substances into particular wells of the microreactor. A) SH-SY5Y cells, previously stained with DiI (red) or CellTracker green (green), respectively, were spotted into wells of the reactor. Fluorescence images show cell distribution directly after the spotting procedure. Scale bar: 500 µm. B) SH-SY5Y cells were differentiated in the microchip and then stained with DiI (red). Subsequently, MitoTracker green (green) was spotted into the central well. Fluorescence images at time points 0 and 5 h incubation at 37 °C are shown. Scale bar: 500 µm.

only applicable for the staining of living cells with membrane-active compounds but should also be possible with hydrophilic substances.

2.3. Cell Culture Experiments

To move forward to culture and differentiation of the neuroblastoma cell line SH-SY5Y in the microreactor, we initially tested a variety of differentiation protocols described in literature in order to identify the best conditions for triggering the formation of long protrusions and high expression levels of differentiation markers. For details, see the experimental procedures, Table S2 and Figures S16 and S17 in the Supporting Information.

To investigate the applicability of the novel reactor for the culture of neuronal cells, differently stained SH-SY5Y cells were cultured in adjacent wells of the microreactor. For this purpose, the cells were stained either with CellTracker (green) or DiI (red) and then distributed with a microdispenser in an alternating pattern into the wells of the reactor (Figure 5A). The results showed only a few wells that contain cells of the wrong color. This is presumably an artifact caused by cross-contamination during the manual transport of the chip to the microscope. Importantly, ink-jet spotted cells were viable and showed a well-spread morphology, as indicated by microscopy analysis on the next day (Figure S12, Supporting Information). Therefore, this experiment clearly demonstrates the possibility of depositing and cultivating different cells in adjacent wells, thus suggesting that the microchip is suitable for more complex cell culture experiments.

Next, the possibility of administrating reagents to differentiated cell populations in a specific well was investigated. For this purpose SH-SY5Y cells were first differentiated inside the microreactor and then stained with the membrane dye DiI. Subsequently, MitoTracker green was added to a single well and the distribution of the dye over time was analyzed (Figure 5B). To this end, 1.5 nL of the dye were added to the 12 nL cell culture media content of the respective well, which corresponds to a dilution of the stock solution of ≈1:10. The relative quantification of the fluorescence signal showed that hardly any dye diffused into the adjacent wells (see also Figure S13D in the Supporting Information). As an additional example to illustrate the potential of the microstructure with respect to cell stimulation in individual wells, we carried out a calcium imaging experiment. To this end, differentiated SH-SY5Y cells in a specific well were treated with the antibiotic ionomycin by inkjet administration. Since ionomycin induces the increase of intracellular calcium levels, the cellular response is detectable by the intracellular fluorogenic sensor dye Fluo-4.[17] As shown in Figure S14 (Supporting Information), the presence of green stained cells in the treated cavity clearly indicates that specific cell stimulation can be performed and the corresponding cellular response can be read out within the microstructure.

We also investigated the prolonged growth and differentiation of SH-SY5Y cells in the microreactor by applying culturing parameters previously optimized in standard culture dishes. The results indicated successful differentiation of cells as well as neuritic protrusions growing through the channel structures, thereby providing cell–cell contacts across adjacent wells (**Figure 6**A). After fixation, staining of the differentiation marker neurofilament−H (NF−H) showed both individual and whole bundles of neuritic protrusions that had grown out of the cells into the channel structures (Figure 6B). Even if no specific staining for neurites was performed, we assume that the observed protrusions are neurites since the images of the differentiated cells (Figures S16.3 and S17, Supporting Information) do not show short tree-like branched projections, but rather long unbranched extensions, typically for neurites.[10]

It is well described in the literature that physical cell–cell contacts influence the differentiation of neuronal cell. Formation of cell–cell contacts leads to upregulation of the expression of gap junction factors and neurotrophic factors, resulting in a higher rate of differentiated cells.[18] Since the cells were randomly distributed in the wells of the microchip, the number of cells in individual wells varied slightly with an average of ≈50 cells per well (Figure S15, Supporting Information). The resulting different cell densities in individual wells can thus influence cell–cell interaction and differentiation. However, to compensate for these differences in later studies, a defined number of cells and even single cells could be deposited by inkjet deposition (see Figure 5).

There is also evidence that neuronal growth is higher within narrow structures than on flat surfaces. Froeter et al. describe a 20-fold increase in the growth rate of cortical neurons within silicon microtubes with a diameter of about 3–4 μm.[19] We assume that this effect also plays a role in our system, since the neuritic protrusions observed during the differentiation studies on flat surfaces only reached lengths of 100–150 μm (see Figure S16 in the Supporting Information), while the protrusions in the microchip had lengths of 200 μm to be able to contact neighboring cells. Furthermore, we rarely observed cells migrating through the channels (less than 1% of all cell soma visible in the microscopy images). Hence, this finding confirms that the design correctly reflects the dimensions typically found in nature for axons and cell protrusions, so that the neurons are prevented from migrating but still allow the formation of cell–cell contacts.

3. Conclusions

In summary, we have established a PDMS microreactor that provides 100 wells for the cultivation, differentiation, stimulation, and analysis of cells. The unique feature of our reactor is the presence of interconnected small channel structures between the wells, allowing the formation of physical cell–cell contacts between cells in adjacent wells, as shown here by the outgrowth of neuronal protrusions. To this end, we have refined the common manufacturing methods for micro stencil masks,[20] so that a simple three-step process can be used to produce thin, two-scale microstructured PDMS layer membranes that can be mounted on glass and loaded with cells.

The mountability of the PDMS microstructure on solid carriers previously patterned with biomolecules is a particular advantage of the reactor design, as it allows the use of complex functionalized surfaces to adjust certain cellular states. The usefulness of such an approach has already been documented

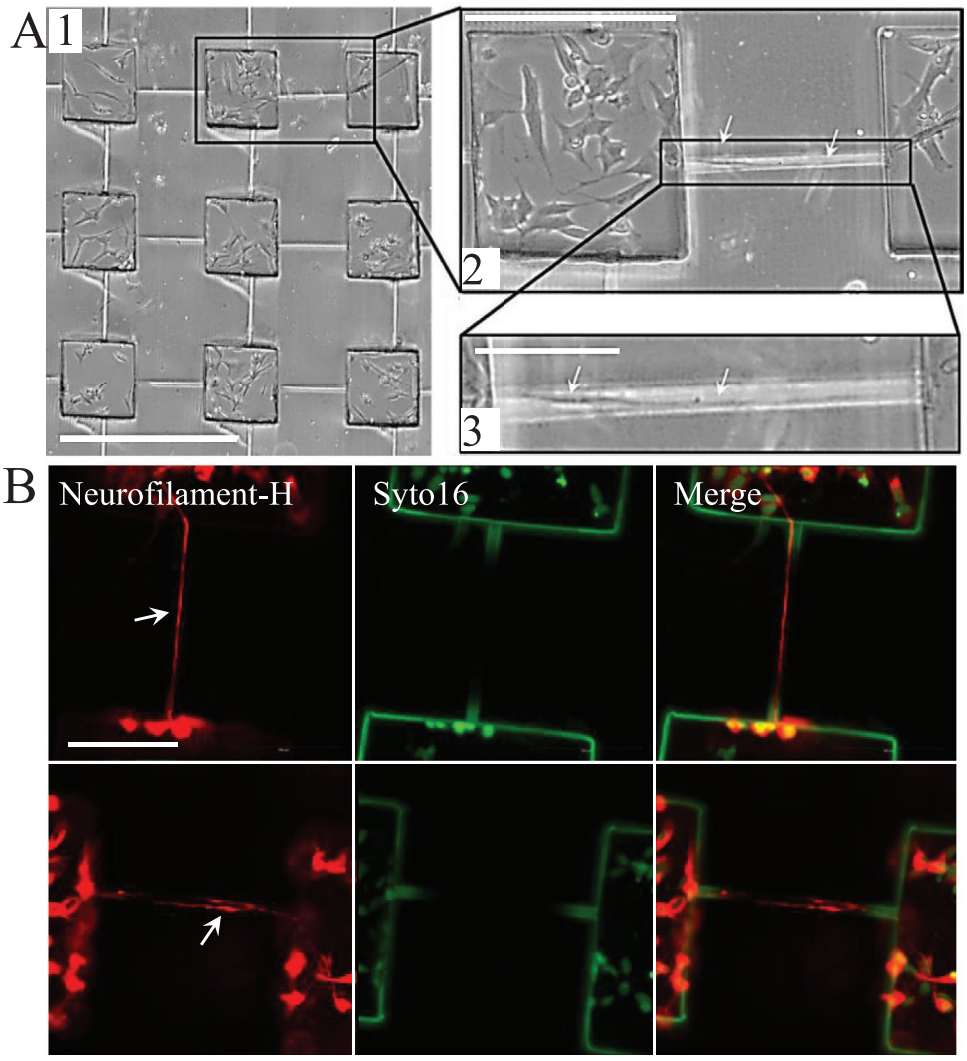

Figure 6. Differentiation of SH-SY5Y cells in the microreactor leads to formation of cell–cell contacts. A) Bright field images of differentiated SH-SY5Y cells in the wells of the microchip. Overview of 9 wells (scale bar: 1) 500 µm, magnification of a well where the connecting channel contains a neuritic protrusion. Scale bars: 2) 200 µm or 3) 100 µm. The arrows depict neuritic protrusion structures. B) Differentiated SH-SY5Y cells, fixed and stained for Neurofilament-H (red) and nuclei (Syto16, green) inside the microreactor. The arrows depict cell protrusions inside the channel structures. Scale bar: 100 µm.

many times with open protein arrays,[21] but the transfer to compartmentalized culture systems, which are needed, e.g., for drug screening, is still difficult. Furthermore, the DNA patterning documented here offers very broad possibilities to integrate nanoscale ligand arrangements into such culture vessels.[15,22] In addition, the mountability of the chip would make it possible to integrate other types of patterns created on the solid support prior to assembly, such as micro- and nanotopographies and even more complex scaffolds that can be produced by laser lithography. Microelectrode arrays/thin film electrodes could also be integrated into such a device to electrically stimulate the cells or to monitor the spontaneous activity of the cells.

As an initial proof-of-concept for the utility of the small connecting channels between the wells, the formation of neuritic protrusions between the cell bodies of spatially separated neuronal cells was demonstrated here. This example shows that it should be possible to stimulate physically separated cells and then study the effect on communication via such cell–cell connections. The cross-sectional area resulting from the width and height of the channels could influence the number of protrusions, but the dimensions should also be suitable for the investigation of other cell lines, as suggested by preliminary experiments with the murine Neuro2a neuroblastoma cell line (data not shown). The chip could also be considered for studying the formation of filopodia, which typically have a length of 5–35 µm and a diameter of 0.2–0.4 µm. By reducing the channel length to 20–30 µm, the chip could therefore become a useful tool to facilitate the microscopic analysis of filopodia, since the movement of these protrusions within closed channel structures is restricted.

Since the reactor enables cell stimulation with soluble reagents as well as the integration of complex cocultures,

comprising, e.g., neurons, glial cells and astrocytes, it could as well be used for the investigation of cellular dysfunction associated with neurodegenerative diseases such as AD. Hence, the here developed microchip could be used as a versatile tool for the systematic investigation of cell–cell communication networks in order to elucidate basic principles relevant for many topics, ranging from biomedical research to synthetic biology.

Supporting Information

Supporting Information is available from the Wiley Online Library or from the author.

Acknowledgements

The authors gratefully acknowledge financial support of this work by the Helmholtz programme BioInterfaces in Technology and Medicine.

Open access funding enabled and organized by Projekt DEAL.

Conflict of Interest

The authors declare no conflict of interest.

Keywords

cell–cell communication, microstructure, neuroblastoma, PDMS

Received: July 27, 2020
Revised: September 25, 2020
Published online:

[1] a) M. Stephenson, W. Grayson, *F1000Research* **2018**, *7*, 517; b) J. Barthes, H. Ozcelik, M. Hindie, A. Ndreu-Halili, A. Hasan, N. E. Vrana, *BiolMed. Res. Int.* **2014**, *2014*, 921905.

[2] a) S. M. Dellatore, A. S. Garcia, W. M. Miller, *Curr. Opin. Biotechnol.* **2008**, *19*, 534; b) R. Peerani, P. W. Zandstra, *J. Clin. Invest.* **2010**, *120*, 60.

[3] a) S. Morelli, S. Salerno, A. Piscioneri, F. Tasselli, E. Drioli, L. De Bartolo, *Chem. Eng. J.* **2016**, *305*, 69; b) J. Penney, W. T. Ralvenius, L.-H. Tsai, *Mol. Psychiatry* **2020**, *25*, 148.

[4] a) C. Soto, *Nat. Rev. Neurosci.* **2003**, *4*, 49; b) G. B. Stokin, L. S. Goldstein, *Annu. Rev. Biochem.* **2006**, *75*, 607; c) L. M. Ittner, J. Gotz, *Nat. Rev. Neurosci.* **2011**, *12*, 67; d) M. A. Busche, S. Wegmann, S. Dujardin, C. Commins, J. Schiantarelli, N. Klickstein, T. V. Kamath, G. A. Carlson, I. Nelken, B. T. Hyman, *Nat. Neurosci.* **2019**, *22*, 57.

[5] M. S. Forman, J. Q. Trojanowski, V. M. Lee, *Nat. Med.* **2004**, *10*, 1055.

[6] a) J. Park, I. Wetzel, I. Marriott, D. Dreau, C. D'Avanzo, D. Y. Kim, R. E. Tanzi, H. Cho, *Nat. Neurosci.* **2018**, *21*, 941; b) J. Park, B. K. Lee, G. S. Jeong, J. K. Hyun, C. J. Lee, S. H. Lee, *Lab Chip* **2015**, *15*, 141; c) P. Miranda-Azpiazu, S. Panagiotou, G. Jose, S. Saha, *Sci. Rep.* **2018**, *8*, 8784.

[7] M. R. Doran, B. D. Markway, I. A. Aird, A. S. Rowlands, P. A. George, L. K. Nielsen, J. J. Cooper-White, *Biomaterials* **2009**, *30*, 4047.

[8] G. A. Hudalla, W. L. Murphy, *Langmuir* **2010**, *26*, 6449.

[9] a) H. Schroeder, B. Ellinger, C. F. W. Becker, H. Waldmann, C. M. Niemeyer, *Angew. Chem., Int. Ed.* **2007**, *46*, 4180; b) R. Meyer, S. Giselbrecht, B. E. Rapp, M. Hirtz, C. M. Niemeyer, *Curr. Opin. Chem. Biol.* **2014**, *18*, 8.

[10] J. I. Forster, S. Koglsberger, C. Trefois, O. Boyd, A. S. Baumuratov, L. Buck, R. Balling, P. M. Antony, *J. Biomol. Screening* **2016**, *21*, 496.

[11] a) K. Wolf, M. Te Lindert, M. Krause, S. Alexander, J. Te Riet, A. L. Willis, R. M. Hoffman, C. G. Figdor, S. J. Weiss, P. Friedl, *J. Cell Biol.* **2013**, *201*, 1069; b) M. Krause, F. W. Yang, M. Te Lindert, P. Isermann, J. Schepens, R. J. A. Maas, C. Venkataraman, J. Lammerding, A. Madzvamuse, W. Hendriks, J. Te Riet, K. Wolf, *Philos. Trans. R. Soc., B.* **2019**, *374*, 20180225.

[12] J. H. George, D. Nagel, S. Waller, E. Hill, H. R. Parri, M. D. Coleman, Z. Cui, H. Ye, *Sci. Rep.* **2018**, *8*, 15552.

[13] C. D. Paul, P. Mistriotis, K. Konstantopoulos, *Nat. Rev. Cancer* **2017**, *17*, 131.

[14] T. Scharnweber, R. Truckenmüller, A. M. Schneider, A. Welle, M. Reinhardt, S. Giselbrecht, *Lab Chip* **2011**, *11*, 1368.

[15] A. Angelin, S. Weigel, R. Garrecht, R. Meyer, J. Bauer, R. K. Kumar, M. Hirtz, C. M. Niemeyer, *Angew. Chem., Int. Ed. Engl.* **2015**, *54*, 15813.

[16] a) L. Nianzhen, M. Schwartz, C. Ionescu-Zanetti, *J. Biomol. Screening* **2009**, *14*, 194; b) J. D. Wang, N. J. Douville, S. Takayama, M. ElSayed, *Ann. Biomed. Eng.* **2012**, *40*, 1862.

[17] K. J. Spinelli, P. G. Gillespie, *PLoS One* **2012**, *7*, e51874.

[18] a) Q. Jiao, X. Li, J. An, Z. Zhang, X. Chen, J. Tan, P. Zhang, H. Lu, Y. Liu, *Front Cell Neurosci.* **2017**, *11*, 200; b) R. Y. L. Tsai, R. D. G. McKay, *J. Neurosci.* **2000**, *20*, 3725; c) B.-T. Tan, L. Wang, S. Li, Z.-Y. Long, Y.-M. Wu, Y. Liu, *Int. J. Clin. Exp. Pathol.* **2015**, *8*, 8129.

[19] P. Froeter, Y. Huang, O. V. Cangellaris, W. Huang, E. W. Dent, M. U. Gillette, J. C. Williams, X. Li, *ACS Nano* **2014**, *8*, 11108.

[20] J. H. Choi, G. M. Kim, *Int. J. Precision Eng. Manuf.* **2011**, *12*, 165.

[21] T. Satav, J. Huskens, P. Jonkheijm, *Small* **2015**, *11*, 5184.

[22] P. Lanzerstorfer, U. Muller, K. Gordiyenko, J. Weghuber, C. M. Niemeyer, *Biomolecules* **2020**, *10*, 540.